# Vacuum flux surfaces produced by inclined coils

Paul E. Moroz
*University of Wisconsin, Madison, Wisconsin 53706 and Lodestar Research Corporation, Boulder, Colorado 80301*

(Received 6 June 1995; accepted 14 July 1995)

The detailed analysis of the vacuum magnetic field structure produced by the inclined toroidal field (TF) coils is presented. This configuration has a potential for adding stellarator properties to the tokamak configuration while maintaining the simplicity of planar coils. Parameters of the system are identified that result in significant stellarator-like effects: large vacuum flux surfaces and appreciable rotational transform. Two sets of closed flux surfaces with opposite helicity are studied: the internal one and the external one. It is found that the external set of flux surfaces possesses a magnetic well and, hence, is favorable for the magnetohydrodynamic (MHD) stability. Also, it has larger enclosed volume and rotational transform. It is, hence, preferential in our studies, in comparison with the internal set that usually features a magnetic hill. Analysis of the flux surface structure and the helical harmonic spectrum yields optimization rules required for the configuration to be of practical interest for possible fusion applications. In a few examples it is demonstrated what occurs if the parameters are set differently than optimal. It is found that toroidal inhomogeneity is a key factor and vacuum flux surfaces disappear in the limit of a very high number of TF coils. The important role of the poloidal field (PF) coil system is stressed, and the possibility of the compensated PF system (with zero total current) is found. © *1995 American Institute of Physics.*

## I. INTRODUCTION

Significant progress in understanding of plasma confinement in various devices, tokamaks, stellarators, reversed field pinches, etc., for the controlled nuclear fusion research has been made in recent years. The major devices for this research were tokamaks. The plasma parameters, obtained in the largest tokamaks—Joint European Torus (JET),[1] Tokamak Fusion Test Reactor (TFTR),[2] JT-60U,[3] and some others, come relatively close to the ones required for the ignition. Nevertheless, a number of key problems still wait their solution for the successful advancement toward a thermonuclear reactor. Among them the most serious ones are the problems of a steady-state (or quasi-steady-state) operation and disruption control.

Tokamaks are intrinsically pulsed devices. The pulse duration depends on limits of the available magnetic flux or Ohmic coil current that must keep growing continuously for the inductive support of plasma current against resistive losses. The flux surfaces in tokamaks are produced by a combination of the toroidal field, generated by toroidal field (TF) coils, and the poloidal magnetic field induced by the plasma current. Poloidal field (PF) coils are also used to correct or change the plasma shape. If the plasma current goes to zero, the rotational transform goes to zero as well, and the flux surfaces disappear. The plasma cannot be confined in a tokamak without plasma current.

Another important type of devices for controlled nuclear fusion research are stellarators. Those are intrinsically steady-state devices where flux surfaces are produced fully by the currents in the external coils. These coils can be mainly of three types.[4,5] One type is the continuous helical windings such as in the stellarators, L-2,[6,7] Uragan-2M,[8] Advanced Toroidal Facility (ATF),[9–11] Heliotron-E,[12] Large Helical Device (LHD).[13] Another type is represented by the modular coils of complicated geometry, such as in the stellarators, Wendelstein VII-AS,[14] Wendelstein VII-X,[15] HSX (Helically Symmetric Toroidal Experiment).[16] The third stellarator configuration used in present-day experiments is the heliac, for example, TJ-II[17] or H-1,[18,19] where TF coils are displaced in such a way that their centers lie on the helical line surrounding a central ring with a current in the toroidal direction and a helical winding. The magnetic field of a heliac, in principle, can be approximated by a modular coil system as well.[20] The purpose of the above discussed various coil systems is to create asymmetry in helical harmonics of the magnetic field, and, as a result, to create a finite rotational transform and closed flux surfaces even without the plasma current (vacuum rotational transform and vacuum flux surfaces).

There are, however, a few serious drawbacks of many stellarator systems. First of all, usually the stellarator coils have rather complicated three-dimensional geometry requiring a high accuracy of assembly. Slight mistakes in the assembly can introduce significant island structures and disturbances to the magnetic surfaces. Second, the confinement properties of the stellarators are normally worse than that of the tokamaks in the case of low collisionality (the banana regime), which is probably the most important regime for the future reactor applications. Third, because of the absence of the Ohmic current, the significant power in RF waves or particle beams will be required for plasma heating to reach ignition.

In this paper we discuss a slight modification of the tokamak coil system. This system possesses the properties of both a tokamak and a stellarator, and has a potential to improve the tokamak conception or extend it. The coil system of this hybrid is the same as the one normally used in tokamaks [it consists of the TF coils and the poloidal field (PF) coils]. The difference, however, is in the vertical inclination of the TF coils. Recently, it was found[21–24] that such a sys-

 1070-664X/95/2(11)/4269/16/$6.00  

tem can be considered as a stellarator (the authors called it "helicofield") because it can produce vacuum flux surfaces with finite rotational transform.

A somewhat similar confinement system, although with the nonplanar TF coils and with the plasma current, has been proposed earlier in Ref. 25. Its main difference from a highly elongated low aspect ratio tokamak is due to equally twisted TF coils (the authors called this device "tokatron" stressing its possible application as a tokamak–torsatron hybrid).

The present paper can be considered as an extension of the analysis of the toroidal confinement system with the planar vertically inclined TF coils toward better understanding its basic principles, configuration optimization, and the potential for applications in controlled fusion.

It is known for many years that vacuum flux surfaces can be produced by the TF coils of special geometry. For example, the planar TF coils of a noncircular cross section placed such that each following coil has an additional turn angle in the poloidal direction,[26,27] can create the vacuum flux surfaces and the vacuum rotational transform. Another important way is the twisting of the TF coils by introducing an additional toroidal modulation of the coil current.[28] Vacuum flux surfaces with a finite rotational transform can also be obtained in a system with the circular planar TF coils whose axes point along the helical line lying on a cylindrical or toroidal surface.[29] Helical axis stellarator configuration with the noninterlocking noncircular planar coils has been considered in Ref. 30.

The vertical inclination of TF coils represents just one and a very simple method of creation of vacuum flux surfaces and rotational transform, and is the subject of detailed studies in the present paper. Because of its simplicity, this method might have a larger potential for fusion applications if a suitable configuration is found.

Some tokamaks, for example, TFTR,[2] have circular TF coils, some of them, for example, Phaedrus-T,[31,32] have rectangular TF coils. Tokamaks built most recently usually have D-shaped TF coils. As an example, the tokamaks JET,[1] Doublet III-D (DIII-D),[33] Alcator C-Mod[34] have D-shaped TF coils. We have checked numerically that coils of various shapes can be vertically inclined to give the effect of the finite vacuum rotational transform. In this paper, however, we have limited ourselves mainly by the TF coils of circular shape, and, in addition, we have introduced some other restrictions on the magnetic configuration of interest, which will be discussed later in this paper. In spite of these limitations, very promising configurations have been found, with the large volume of the closed flux surfaces and significant vacuum rotational transform.

There are a few possible advantages of using inclined coils in a tokamak. Among them are the non-Ohmic start-up of the discharge (up to the high plasma density) that saves the valuable magnetic flux of the Ohmic current transformer and improves durability of the construction of the tokamak. Some other applications can be related to the problem of disruption control[35–38] via the helical harmonic components, or to the problem of minimizing the magnetic field forces on the TF coils.[39]

Because of additional rotational transform produced by the inclined coils, the device considered can be operated at lower plasma currents (for the same safety factor values). That means the reduction of energy released during disruptions and prolonged discharge operation (less Ohmic current is necessary). Also, the savings in the current drive power (required for the steady-state operation) can be significant.

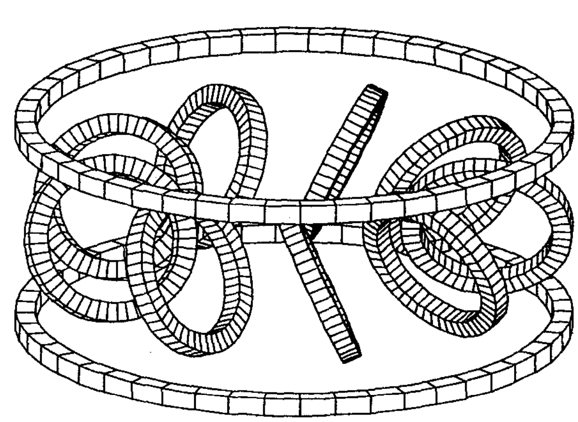

FIG. 1. Scheme of the simplest device with inclined TF coils and two PF rings.

The paper is organized as follows. In Sec. II, the coil system under consideration is described, and the results of calculations representing all major effects are given. The role of the PF coil system is discussed in Sec. III. Two separate sets of closed flux surfaces are under discussion in Sec. IV. Variation of the system properties caused by changing of its main parameters is considered in Sec. V. The rules for configuration optimization and the scaling laws are given in Sec. VI. The discussion and main conclusions are presented in Sec. VII. The numerical code, UBFIELD, used in our calculations, is described briefly in the Appendix.

## II. A DEVICE WITH VERTICALLY INCLINED TF COILS

The simplest device with the system of vertically inclined TF coils is shown in Fig. 1. This particular example considers nine circular coils with the diameter of 0.80 m each, placed evenly along a torus with a major radius of 1.0 m. The angle of the vertical inclination is 0.4 rad. Inclined TF coils produce a net vertical magnetic field. To compensate this field we included two PF rings with radii of 1.4 m, one above and one below the TF coils, with the vertical distance between them of 1.1 m. The currents in the TF coils were 250 kA and currents in PF coils were 115 kA.

The resulting flux surfaces are presented in Figs. 2(a)–2(c) for the three principally different cross sections. The numerical code, UBFIELD, and the numerical technique used in these calculations are described briefly in the Appendix. The last flux surface has a volume of 0.047 $m^3$ (the average minor radius is about 0.135 m).

As one can see, the simple case considered is already interesting. First, there is a system of closed flux surfaces with the significant volume. Second, the flux surfaces does not go beyond the coils, so one can easily enclose them into the simple toroidal vacuum chamber, the same as in tokamaks. Third, the vacuum rotational transform is significant, it

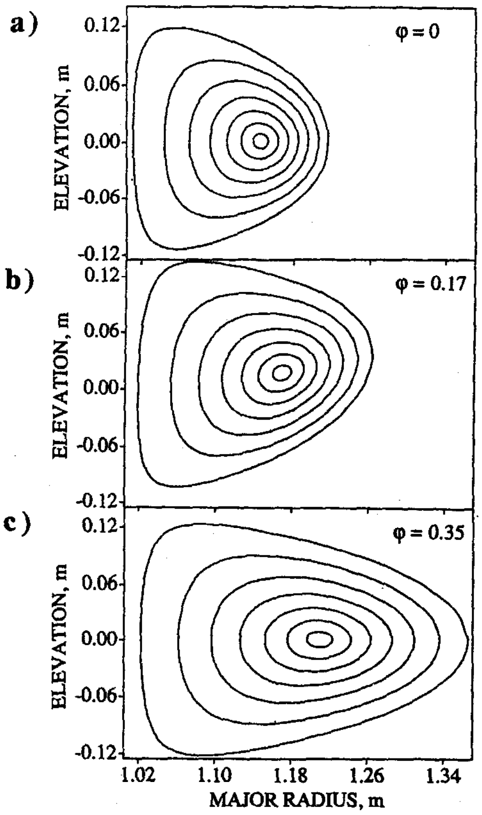


FIG. 2. External set of the closed flux surfaces for the device of Fig. 1 at three cross sections: (a) at the toroidal position of TF coils, (b) at one-quarter of the toroidal period, and (c) at one-half of the toroidal period, i.e., between the TF coils.

varies from $\iota$=0.29 in the center to $\iota$=0.16 at the edge, corresponding to the safety factors $q=3.4$ in the center to $q=6.0$ at the edge. The rotational transform dependence on the average minor radius of the flux surface is shown in Fig. 3.

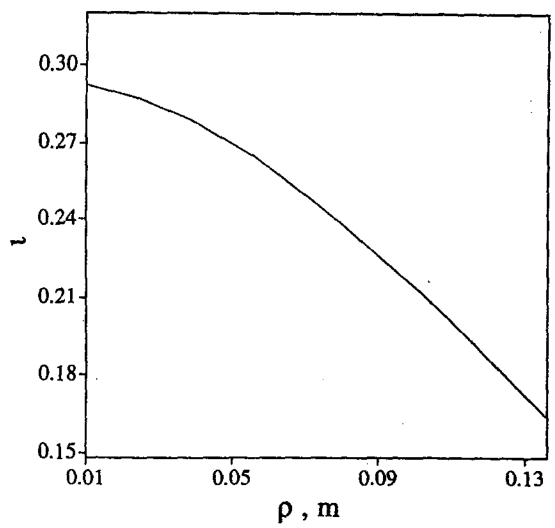


FIG. 3. Rotational transform versus minor radius for the device of Fig. 1.

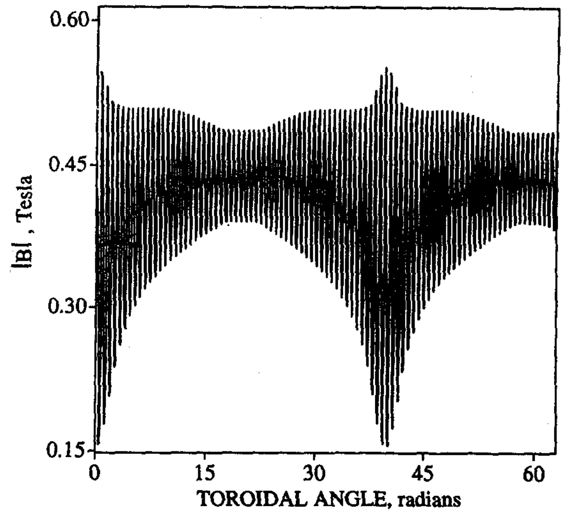


FIG. 4. Variation of $|B|$ along the field line for the device of Fig. 1.

The major drawback of the considered system is the significant ripple of the magnetic field. The variation of $|B|$ along the field line for the last flux surface is shown in Fig. 4, and dependence of the magnetic ripple,

$$\eta(\rho)=\frac{B_{\max}-B_{\min}}{B_{\max}+B_{\min}}, \tag{1}$$

on the average minor radius, $\rho$, is given in Fig. 5.

One more characteristic of the flux surfaces of the above example is the spatial magnetic axis that is represented by a helical line along the torus [see Figs. 2(a)–2(c)]. This peculiarity is usual for many stellarator configurations as well.

It is important to note, also, that the magnetic configuration obtained is favorable for MHD stability. It possesses a magnetic well, which can be defined through the integral

$$U=\int \frac{dl}{B}, \tag{2}$$

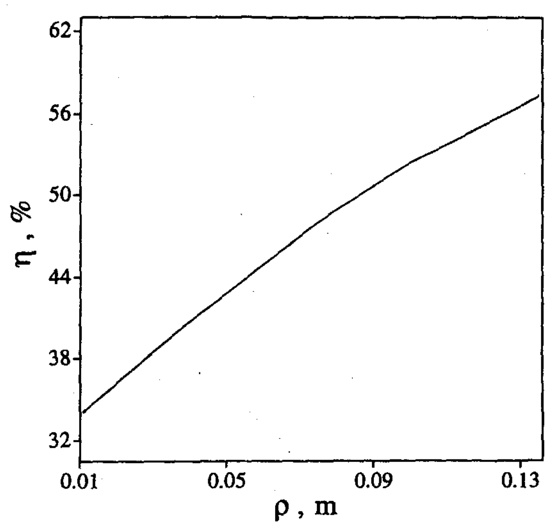


FIG. 5. Magnetic field ripple versus minor radius for the device of Fig. 1.

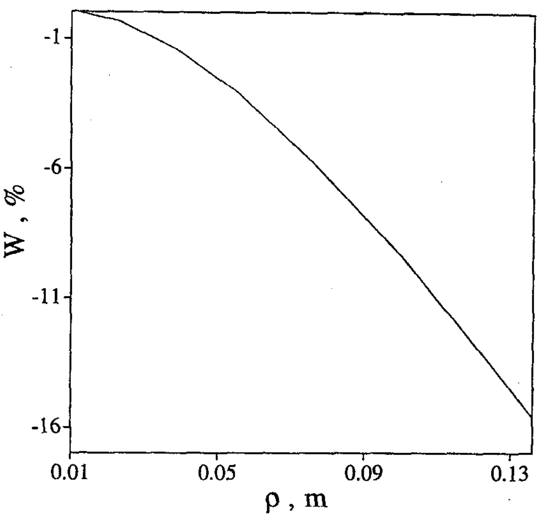


FIG. 6. Radial variation of the magnetic well for the device of Fig. 1.

taken along the field line and averaged over the flux surface. Such an averaged integral, $U$, can be expressed through the derivative of the enclosed volume, $V$, over the enclosed toroidal magnetic flux $\Psi$,[40]

$$\langle U\rangle = \frac{dV}{d\Psi}. \tag{3}$$

The magnetic configuration is favorable to MHD stability if $\langle U\rangle$ decreases with the minor radius, $\rho$. The relative deepness of the magnetic well can be defined as the ratio

$$W(\rho) = \frac{\langle U(\rho)\rangle - \langle U(0)\rangle}{\langle U(0)\rangle} = \frac{V'[\Psi(\rho)] - V'(0)}{V'(0)}, \tag{4}$$

where $U(0)$ and $V'(0)$ correspond to the values near the magnetic axis, and $U(\rho)$ and $V'[\Psi(\rho)]$ to the values for the given flux surface with the average minor radius, $\rho$. Figure 6 shows the dependence of $W(\rho)$ that corresponds to the total magnetic well of about $W_t = 16\%$.

Many characteristics of the flux surfaces considered above are typical for the stellarators: vacuum flux surfaces and vacuum rotational transform, spatial magnetic axis, and different cross-section shapes at different toroidal locations. On the other hand, the diminishing of the rotational transform with the minor radius is a typical characteristic of the tokamaks and is very rare in stellarators.

In the following analysis we will try to understand why the above system is working, and how the magnetic configuration can be optimized to increase the enclosed volume, to decrease the magnetic ripple, or to increase the vacuum rotational transform. It was found, however, that such optimizations often contradict one to another, and compromises have to be found. For example, the optimization directed at increasing of the enclosed volume, under the constraint that it still has to be kept inside the TF coils, usually pushes the plasma closer to the TF coil center, and, at the same time, decreases the rotational transform. Large rotational transform is important for the high stability $\beta$ limit and equilibrium $\beta$ limit of the plasma. We speculate that rotational transforms below $\iota=0.1$ are not enough for the good plasma confinement. However, this point has to be checked in experiments, and if lower values of $\iota$ are acceptable then the further optimization is possible.

## III. IMPORTANCE OF THE CORRECT PF COIL SYSTEM

So far, the PF coil system considered was very simple. It included just two rings: one above and one below the equatorial plane. Nevertheless, the magnetic configuration had many attractive properties discussed above. However, this configuration easily loses its attractiveness if the parameters of the system (i.e., coil positions, coil sizes, or current magnitudes) are slightly changed.

For example, one can try to increase the enclosed volume by varying the ratio of the PF coil current to the TF coil current. For the case of the current in PF coils, $I_{\mathrm{PF}}=105$ kA (all other parameters are the same as above), the volume inside the last flux surface has increased significantly to 0.168 $\mathrm{m}^3$. Rotational transform has increased to $\iota(0)=0.55$ at the magnetic axis and $\iota(a)=0.16$ at the separatrix, with $\rho=0.25$ m. Those are positive changes. However, at the same time there are a few negative changes as well. Among them is strong increase of magnetic ripple that varies from 50% at the axis to 85% at the separatrix. Also, the flux surfaces now go significantly beyond the TF coils, and hence the vacuum chamber cannot be a simple toroid, as before, but has to accommodate the complicated shape of the flux surfaces. In spite of the fact that many present-day stellarators have complicated vacuum chambers corresponding to the flux surface geometry, we consider this as a serious drawback of the system and prefer to avoid such situations.

In the opposite case of higher $I_{\mathrm{PF}}=123$ kA, the ripple decreases to 18% at the separatrix and the flux surfaces keep well inside the TF coils. However, the useful volume became so small, $V=0.005$ $\mathrm{m}^3$, that this case is not of interest.

These two examples were intended to demonstrate that while the PF system includes just two rings, the improvement of the flux surface structure is very limited. Also, it is clear that the configuration of the closed flux surfaces, that satisfy our constraints, exists only in a relatively small region of currents.

Similar calculations, carried out for many various cases, show that distribution of the current in the PF coil system around the TF coils can help a lot in controlling the flux surface configuration and obtaining better parameters. These results are based on the consideration of PF coil system configurations consisting of four, six, eight, or ten rings distributed around the TF coils. The following example is intended to demonstrate this effect. For simplicity, we considered the case when each PF ring carried the same current.

The six-ring configuration chosen for the demonstration is presented in Fig. 7. The last closed flux surface is shown as well. The currents in the inclined TF coils were the same as before, and currents in the PF rings were 46 kA each. These currents have been chosen such that the flux surfaces obtained were well confined inside the TF coils, and, hence, the simple toroidal vacuum chamber could be used. The spatial location of the PF rings has been chosen such that the

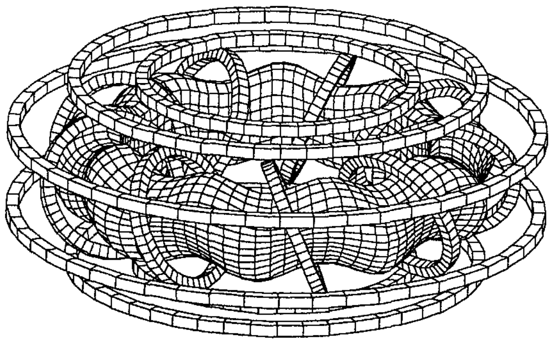

FIG. 7. Configuration with nine inclined TF coils and six PF rings. The last closed flux surface is shown as well.

standard horizontal and vertical ports of the vacuum vessel can be easily accessible and not blocked by the rings. The location of PF rings is shown in Fig. 8 by the squares. Two cross sections of the last closed flux surface, at the toroidal position of TF coils (solid curve) and between the TF coils (dashed), are given as well.

The system of closed flux surfaces obtained is shown in Figs. 9(a) and 9(b) for the two cross sections, at the toroidal position of TF coils and between the TF coils, respectively. The main changes in comparison with the previous case (see Fig. 2) are the following. The enclosed volume has almost tripled and reached $V=0.14$ m$^3$, and the average minor radius is about 0.24 m. The flux surface's location became more central relative to the TF coils.

Also, the flux surfaces have now the typical vertically elongated shapes. The magnetic axis is still spatial. However, its horizontal displacement is only 5 cm, from $R=1.11$ m at the toroidal position of TF coils to $R=1.16$ m in the cross section between TF coils. The rotational transform varied

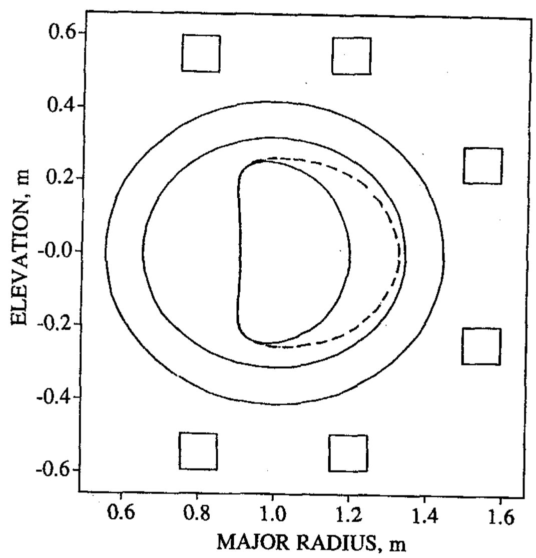


FIG. 8. Projection of the coil system of the device of Fig. 7 on the poloidal cross section, and the last closed flux surface at the toroidal position of TF coils (solid curve) and between TF coils (dashed).

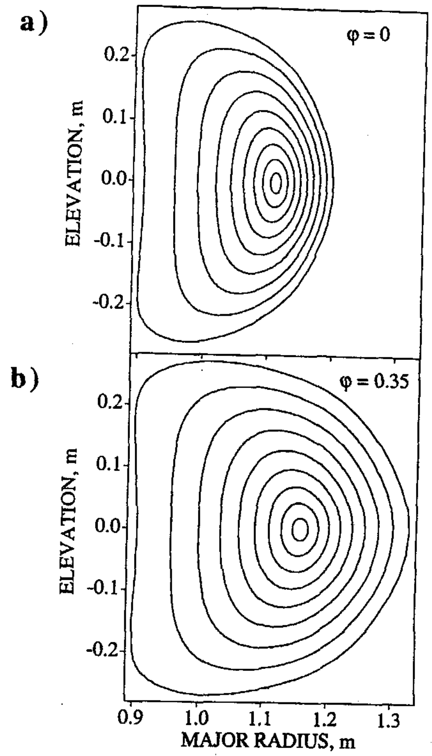


FIG. 9. External set of the closed flux surfaces for the device of Fig. 7 at the cross sections corresponding to the toroidal position of TF coils (a), and between the TF coils (b).

from $\iota=0.18$ in the center to $\iota=0.11$ at $\rho=0.24$ m. The total magnetic well was $W_t=22\%$. The magnetic ripple has varied from $\eta=25\%$ in the center to $\eta=58\%$ at the edge.

In the cases considered above, the significant total current has been carried by the PF coil system. This current has been varied from $I_{\rm PF}=230$ kA for the case of two rings, to $I_{\rm PF}=276$ kA for the case of six rings. In a tokamak, however, the net current in the PF rings might interfere with the performance of the Ohmic current transformer.

In the following example, we would like to show that the PF system can be compensated such that the total current $I_{\rm PF}=0$. The TF coil system chosen for the demonstration consisted of nine inclined coils, the same as before. The locations of eight rings of the PF system are shown by the squares in Fig. 10, giving projection on the poloidal cross section. We just added two additional rings at the major radius, $R=0.45$ m, each carrying the negative current, $I=-132$ kA, to compensate the positive current of other rings ($I=44$ kA each). Two cross sections of the last closed flux surface, at the toroidal position of TF coils and between the TF coils, are presented in Fig. 10 by solid and dashed curves, respectively, as well. The volume, enclosed by the last flux surface, was $V=0.1$ m$^3$, and the total magnetic well was $W_t=12\%$. The magnetic ripple has varied from $\eta=25\%$ in the center to $\eta=49\%$ at the average minor radius of $\rho=0.195$ m. The rotational transform has varied from $\iota(0)=0.18$ at the magnetic axis to $\iota=0.13$ at the edge. Hence, the ripple and rotational transform have not been effected by compensation.

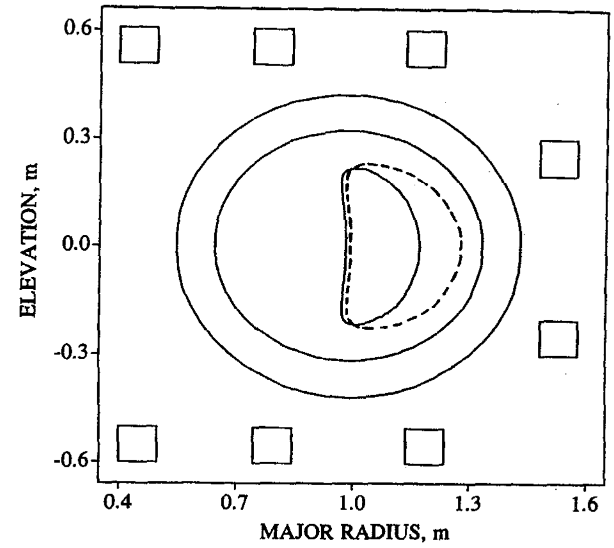


FIG. 10. Poloidal projection of the coils for the device with the compensated PF coil system. Cross sections of the last closed flux surface at the toroidal position of TF coils (solid curve) and between TF coils (dashed) are shown as well.

However, the minor radius of the last closed flux surface has decreased.

Figure 10 shows also that the flux surfaces are localized close to the TF coil center, and are well confined inside the TF coils. Summarizing, the flux surfaces produced in the device with the compensated PF system, although slightly worse than without compensation, still are of interest and basically satisfy our main constraints.

## IV. TWO SETS OF CLOSED FLUX SURFACES

So far we have presented the results only for the main set of closed flux surfaces—the external one. However, at the same parameters there is another set of closed flux surfaces that exists simultaneously with the external one, but at smaller major radii. We call this set the internal one. This phenomenon has been found in the earlier publication[22] as well. In this section we are studying this internal set to clarify its role.

Let us consider the same device with the same currents as presented in Fig. 7, but this time we will look for the internal set of flux surfaces. Figures 11(a) and 11(b) show two cross sections, at the toroidal position of TF coils and between TF coils, of the flux surfaces found. The volume enclosed by the last flux surface is still significant, $V=0.024$ m$^3$, and the rotational transform is relatively high, $\iota=0.19$ at the magnetic axis and $\iota=0.145$ at $\rho=0.12$ m. The magnetic ripple varies from $\eta=20\%$ at the magnetic axis to $\eta=39\%$ at $\rho=0.12$ m. The perspective view of the last closed flux surface together with inclined TF coils is shown in Fig. 12.

Analysis of many similar cases led us to the following conclusion. Although the simultaneous existence of two separate sets of closed flux surfaces is an interesting phenomenon, not found in tokamaks or stellarators, the internal set, probably, will have less practical importance. It is not only because the enclosed volume is notably smaller than that for the external set, but mostly because the flux surface configuration features a magnetic hill, which is unfavorable for the MHD stability. While the total magnetic well was $W_t=22\%$ for the external set, it was negative, $W_t=-18\%$, for the internal one in the examples discussed.

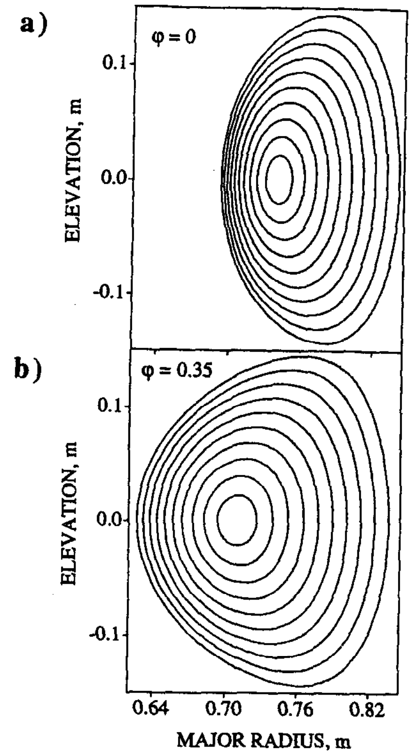


FIG. 11. Flux surfaces from the internal set for the device of Fig. 7: (a) at the toroidal position of TF coils; (b) between TF coils.

Two sets of the closed flux surfaces, internal and external, described above in Sec. V have opposite helicity. This means that the main helical harmonics for these two sets are opposite. To come to this conclusion, we have analyzed the Fourier spectrum for the last flux surfaces for each set.

We have utilized a coordinate system that has its origin at the spatial magnetic axis. Then the flux surfaces have been

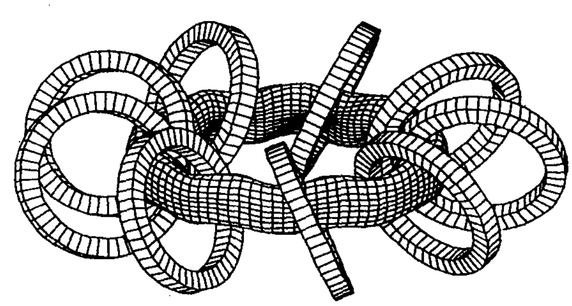

FIG. 12. Perspective view of the last closed flux surface of the internal set for the device of Fig. 7.

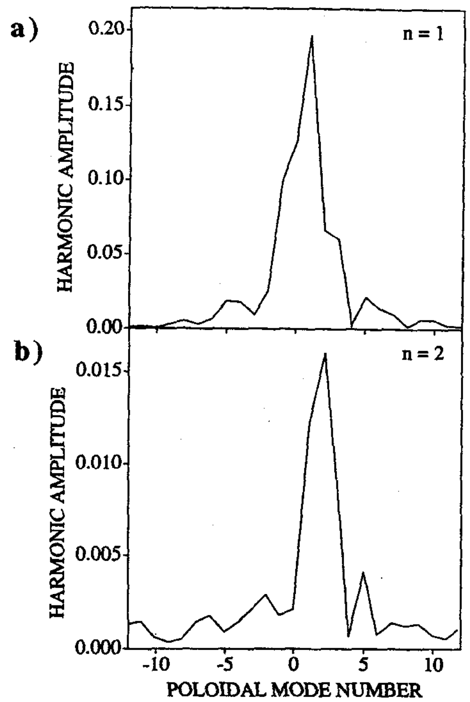


FIG. 13. Helical harmonic spectrum of the last closed flux surface from the external set for the device of Fig. 7 for $n=1$ (a) and $n=2$ (b).

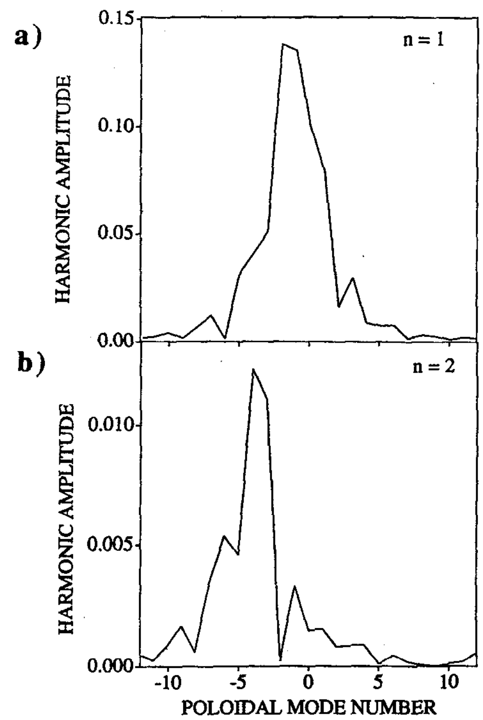


FIG. 14. Helical harmonic spectrum of the last closed flux surface from the internal set for the device of Fig. 7 for $n=1$ (a) and $n=2$ (b).

described in terms of minor radius, $\rho$, as a function of poloidal, $\vartheta$, and toroidal, $\varphi$, angles: $\rho=\rho(\vartheta,\varphi)$. This function, $\rho$, has been expanded into the helical harmonics,

$$\rho(\vartheta,\varphi)=\sum_m \sum_n C_{nm}\cos(nN\varphi+m\vartheta). \tag{5}$$

The coefficients, $C_{nm}$, can be calculated by integrating $\rho(\vartheta,\varphi)$ in the poloidal and toroidal directions:

$$C_{nm}=\frac{N}{2\pi^2}\int_{-\pi/N}^{\pi/N} d\varphi \int_{-\pi}^{\pi} d\vartheta \rho(\vartheta,\varphi)\cos(nN\varphi+m\vartheta). \tag{6}$$

In the above expressions, $N$ is the number of magnetic field periods along the torus, that is equal to the number of the inclined coils, and $n$ and $m$ are integers.

The amplitudes of the positive helical harmonics, given by $|C_{nm}|$ for $n$ and $m$ positive, and negative helical harmonics, given by $|C_{nm}|$ for $n$ positive and $m$ negative, calculated for the external and internal sets of flux surfaces, considered in Sec. V, are presented in Figs. 13(a) and 13(b) and 14(a) and 14(b), respectively. Also, we have normalized all coefficients to the $C_{00}$. There can be also harmonics with $n=0$, $m\neq 0$ (because of toroidicity, for example). However, these are not the helical harmonics and not related to the stellarator properties of the device. Figures 13(a) and 14(a) show helical harmonics for the main toroidal wave number, $n=1$, while Figs. 13(b) and 14(b) show the most important satellite harmonics for $n=2$. As one can see, the set of inclined coils effectively creates asymmetry in helical harmonics. Thus, for the external set of the flux surfaces, the positive helical harmonics have larger amplitudes, while for the internal set the negative helical harmonics are larger.

The correctness of the helical harmonic amplitudes obtained has been checked in the code by recalculating the flux surfaces by using Eq. (5). The agreement with the original flux surfaces was excellent.

Here we have presented helical harmonics for decomposition of the minor radius $\rho$. Some other quantities, for example $|B|$ on a flux surface as a function of poloidal and toroidal angles, can be expanded into helical harmonics as well. The results are similar: the external and internal sets of flux surfaces have opposite helicity.

## V. VARIATION OF THE MAIN PARAMETERS

Optimization of the system can be obtained by varying its parameters. Because of the conclusion made in Sec. V, the main attention in the following will be paid to the external set of closed flux surfaces.

First we present the results on variation of the primary parameter leading to the finite rotational transform—the angle of vertical inclination of TF coils. The number of coils and their locations are kept the same as in example presented in Fig. 7. The fact that flux surfaces exist if currents in PF rings vary approximately in direct proportion with the angle of vertical inclination of TF coils, $\gamma$, significantly simplifies these studies. The results are summarized in Figs. 15–18.

Figure 15 shows how the rotational transform, $\iota$, increases with the angle of vertical inclination of TF coils, $\gamma$.

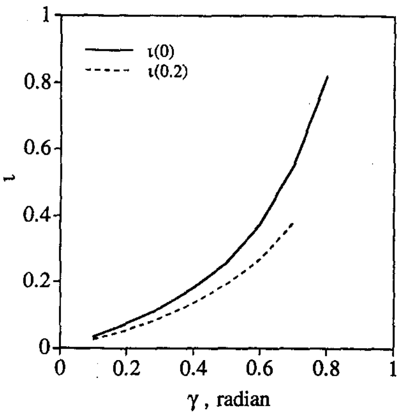


FIG. 15. Rotational transform versus the angle of inclination.

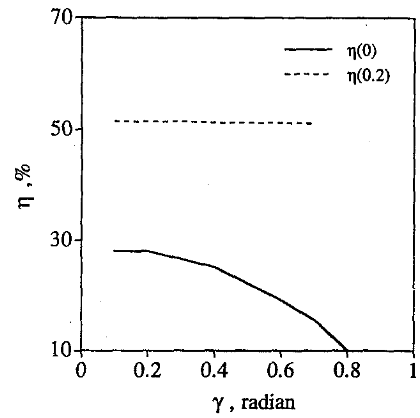


FIG. 17. Magnetic ripple versus the angle of inclination.

One can see the fast growth of $\iota(0,2)$, the rotational transform at $\rho=0.2\ m$, and $\iota(0)$, the rotational transform at the magnetic axis.

This growth of $\iota$ can be related to growth of the helical harmonic amplitudes, which are shown in Fig. 16 for the basic toroidal wave number, $n=1$, and poloidal numbers, $-2\leqslant m\leqslant 2$. The growth of $\iota$ at small angles of inclination, $\gamma<0.5$ rad, approximately corresponds to the growth of the strongest helical harmonic, $C_{1,1}$, while at high angles, $\gamma>0.5$ rad, it corresponds to the growth of the helical harmonic, $C_{1,2}$, which is the strongest at high $\gamma$.

When there is no inclination of TF coils, $\gamma\rightarrow 0$, all helical harmonics disappear. Among harmonics considered in Fig. 16 only $C_{1,0}$ is still presented. It corresponds to the periodic variations due to the finite number of TF coils. This harmonic is responsible for the standard magnetic ripple in a tokamak. It is interesting to see that its amplitude decreases significantly with increasing $\gamma$.

The ripple at the magnetic axis decreases substantially with increasing $\gamma$ as well. This can be seen from the solid curve in Fig. 17. Nevertheless, the magnetic ripple at $\rho=0.2$ m (dashed curve) did not change notably with $\gamma$.

The volume enclosed by the last flux surface varies with $\gamma$ as well (see Fig. 18). It is relatively large for $\gamma$ up to $\gamma\approx 0.6$, and then drops quickly when $\gamma$ increases further. The maximum volume corresponds to $\gamma=0.4$. Thus, the system shown in Fig. 7 represents the optimization over the enclosed volume. The rotational transform is still high enough. If one would like to make optimization of the rotational transform then, probably, one has to choose $\gamma=0.6$.

In a tokamak, a large number of TF coils is normally used to avoid the magnetic ripple produced by toroidal inhomogeneity. In configurations with vertically inclined TF coils, the stellarator-like vacuum rotational transform and closed flux surfaces are produced. It is not clear, however, how the number of TF coils can effect this phenomenon. In particular, it is not clear if the configuration with the large number of inclined TF coils remains stellarator properties.

In the following we consider the same coil configuration as in our previous example (Fig. 7). This time, however, the number of TF coils, $N$, is varied. Because of variation of $N$, to keep the balance between the vertical magnetic fields produced by the inclined TF coils and PF rings, it was necessary to change the current in the TF coils approximately in the reversed proportion with $N$. Moreover, the coil current was fine tuned to obtain the maximum volume of the enclosed flux surfaces while keeping these surfaces inside the TF coils. Our results are summarized in Figs. 19–23.

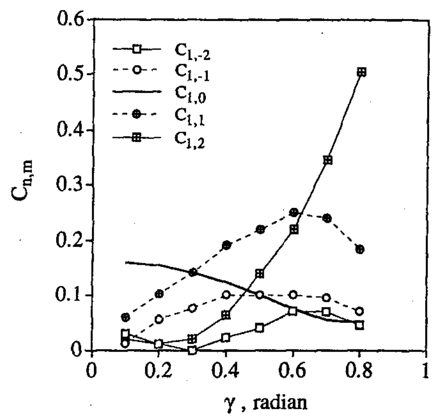


FIG. 16. Helical harmonic amplitudes versus the angle of inclination.

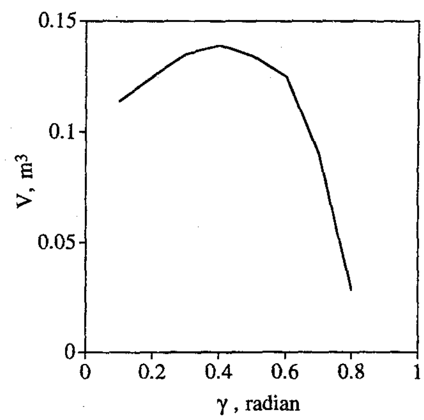


FIG. 18. Enclosed volume versus the angle of inclination.

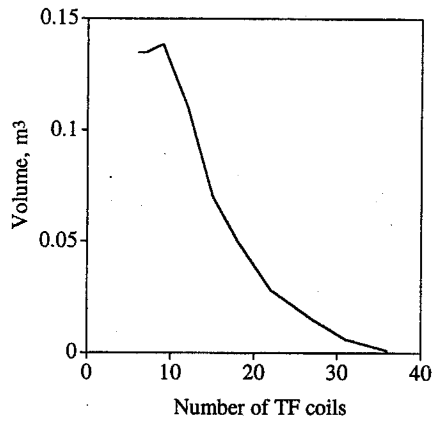


FIG. 19. Enclosed volume versus the number of TF coils.

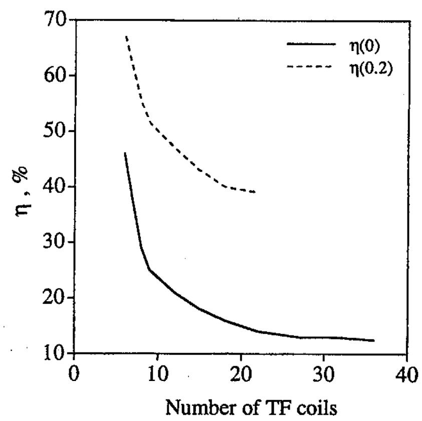


FIG. 21. Magnetic ripple versus the number of TF coils. Solid curve—at the magnetic axis; dashed—at $\rho$=0.2 m.

Figure 19 gives the volume enclosed by the last flux surface as a function of $N$. At high $N$ ($N>10$ for our case), the enclosed volume decreases quickly with increasing $N$, and flux surfaces practically disappear at very high $N$, for our case at $N>36$. Thus, toroidal inhomogeneity is a key factor for the configuration with inclined TF coils.

An important effect of the flux surface displacement has been observed in these calculations. While the number of TF coils was relatively small, closed flux surfaces were located near the TF coil center. This central location is important for many possible applications where the flux surfaces are required to be far enough from the current carrying parts. However, an increase of the number of TF coils causes the shift of flux surfaces in the direction of larger major radius and closer to the outside current filament of the TF coil [similar, the flux surfaces from the internal set (see Sec. V for details) move inward toward the inner current filament of the TF coil and farther from the coil center]. When $N$ is very high, the flux surfaces exist only in a small neighborhood of the current filaments of the coil, and the enclosed volume is very small. Figure 20 demonstrates this effect by showing the magnetic axis displacement from the TF coil center versus the number of TF coils. The solid line is for the poloidal cross section at the toroidal position of TF coils, and the dashed line is for the cross section toroidally located between the coils. One can see that at low $N$ there is significant variation of the magnetic axis location depending on the cross section chosen, while at high $N$ this variation is small.

Magnetic ripple is an important factor for plasma confinement in the device. Figure 21 shows the magnetic ripple at the axis, $\eta(0)$, and at the average minor radius of 0.2 m, $\eta(0.2)$, as a function of the number of TF coils. One can see that magnetic ripple decreases with increasing $N$, similar to that in a tokamak. It is important to note that for low $N$ ($N<9$ in our case) there is a sharp increase of the magnetic ripple. Thus, low $N$ has to be avoided because of the very large ripple. In the case considered, the magnetic ripple was still significant for very large $N$. This effect is because of the flux surfaces move closer to the current filaments when $N$ increases.

Analysis of the rotational transform variation shows following dependencies. Rotational transform at the magnetic axis stays approximately the same ($\iota\approx 0.2$) for $N$ in the range between 8 and 23 (Fig. 22). It increases with $N$ at high $N>23$. However, one has to remember that at $N>23$ the enclosed volume decreases quickly with $N$ (see Fig. 19), thus

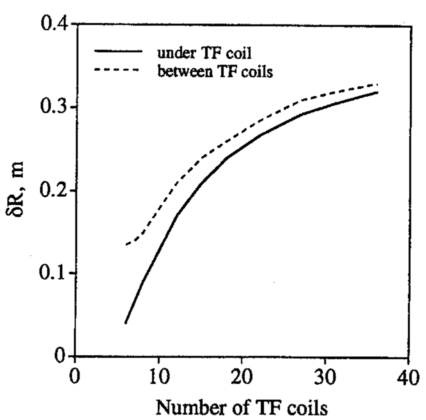


FIG. 20. Magnetic axis displacement versus the number of TF coils. Solid curve—at the toroidal position of TF coils; dashed—between TF coils.

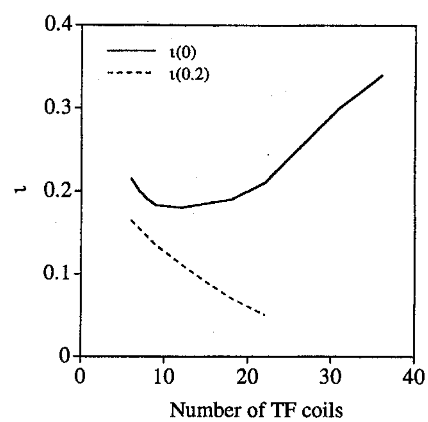


FIG. 22. Rotational transform versus the number of TF coils. Solid curve—at the magnetic axis; dashed—at $\rho$=0.2 m.

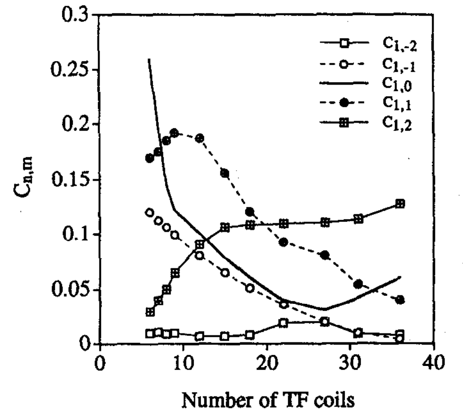


FIG. 23. Helical harmonic amplitudes versus the number of TF coils.

making this fact of no practical interest. The rotational transform at $\rho$=0.2 m is shown in Fig. 22 by the dashed curve. It generally decreases with $N$ in the range of $N$ considered.

The behavior of main helical harmonics is presented in Fig. 23. The same harmonics as in Fig. 16 are considered. It is important to note that at low $N$ the $C_{1,1}$ harmonic is the strongest among helical harmonics, while at high $N$ the strongest is $C_{1,2}$. The constraint taken that $\iota$ has to be larger than 0.1 inside the enclosed volume, imposes a strong limitation on acceptable $N$ (see Fig. 22), which hence cannot be too large.

Results presented in this section clearly show that the number of TF coils is a very important factor. The configuration discussed was optimal for $N$ around 9. Of course, for a different set of parameters of the device a different number of TF coils will be optimal. This section was intended just to show that there is some optimal $N$, and to show how the various important factors, such as enclosed volume, flux surface location, rotational transform, magnetic ripple, etc., change with $N$. The closed flux surfaces disappear in the limit of very high number of TF coils. Thus, toroidal inhomogeneity is a key factor. Inclination of TF coils alone cannot create closed flux surfaces until there is definite level of toroidal inhomogeneity in the system.

## VI. CONFIGURATION OPTIMIZATION

In the previous sections it was shown that there are some special parameters of the coil system when the magnetic structure can be called an optimal one. Let us formulate more explicitly of what are our criteria for the optimal magnetic structure.

(1) Large enclosed volume: the volume enclosed by the last flux surface has to be as large as possible, and not much less than the volume of the simple toroid enclosed by the TF coils.

(2) Large rotational transform: the vacuum rotational transform of the magnetic configuration has to be appreciably high so it can be used for the effective plasma confinement. We have put the limit, $\iota$=0.1, and require that the rotational transform was higher than that limit everywhere inside the enclosed volume.

(3) Low magnetic ripple: the magnetic ripple has to be as low as possible. This ensures better plasma confinement.

(4) Central location of the last closed flux surface: the flux surfaces obtained have to be well confined inside the TF coils, and even between the TF coils should not go beyond the coil radius. Then a simple toroidal vessel (similar to the one used for a standard tokamak) can be utilized for the plasma experiments.

(5) Central location of the magnetic axis: the magnetic axis of the configuration has to be as close to the TF coil center as possible, and as far from the current carrying parts of the TF coil as possible. This requirement is different from the previous one: in some cases the last flux surface has a rather central location, but the magnetic axis location is strongly nonsymmetric and close to the current filament. This requirement simplifies various applications of the proposed scheme for plasma confinement. Indeed, normally there is a vacuum chamber inside the TF coils that require some distance from the current filaments. Then, in case of a magnetic axis location close to the current filaments of TF coils the significant part of useful plasma volume can be lost. Also, the strongly nonsymmetric location of the magnetic axis means very high spatial gradients of density and temperature of the plasma. In this case the particle and energy losses are high.

(6) Significant magnetic well: the magnetic configuration has to be magnetohydrodynamically (MHD) stable. Thus, we require the configuration to possess a strong magnetic well that is favorable for MHD stability.

These are our main requirements. It is not an easy task to satisfy all of them simultaneously, and often an attempt to optimize the configuration on one particular requirement contradicts to some other requirement. Thus, usually the compromise configuration can be found that satisfies all above requirements, but only to some degree.

A lot of calculations have been carried out in an attempt to find an optimal configuration that satisfies the six main requirements listed above. Our major findings can be formulated as three rules. These rules although do not represent the full set of conditions, are helpful in finding the configuration close to the optimal one. In our calculations, these rules have been always satisfied for the best cases when the magnetic configurations have been close to optimal.

### A. Rule 1 (the optimization rule)

The major radius of the TF coil, $R$, the number of inclined TF coils, $N$, the angle of inclination, $\gamma$, and the diameter of the TF coil, $D$ (for the more general case of noncircular TF coils it will be an effective vertical size of the coil), are not independent parameters but have to satisfy the following simple relation:

$$\xi \equiv \frac{DN \sin \gamma}{\pi R} \approx 1. \tag{7}$$

Thus, if one will change major radius, $R$, or number of TF coils, $N$, or their size, $D$, or inclination angle, $\gamma$, simultaneously in such a way that the parameter $\xi$ stays close to 1, the configuration will be close to optimal. For the quantita-

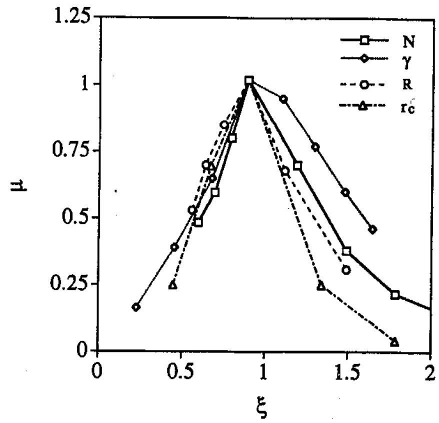


FIG. 24. Demonstration of the "optimization rule" and the scaling law. Dependence of the aiming parameter, $\mu$, vs $\xi$ is presented for variations of $N$, $\gamma$, $R$, and $r_c$.

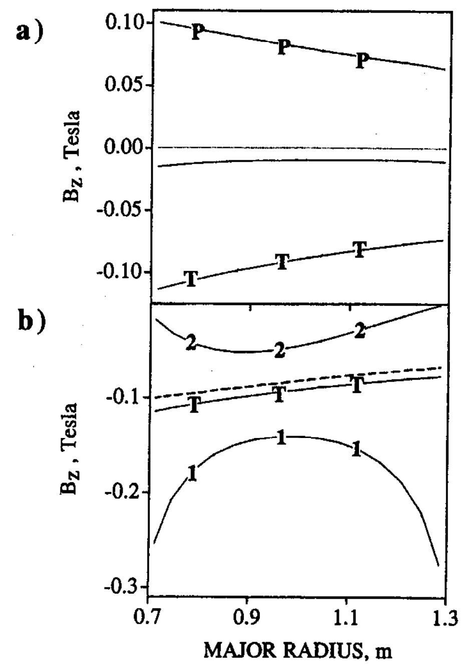


FIG. 25. Demonstration of the "balance rule" for the vertical magnetic field. The following vertical magnetic field components are shown: (a) toroidally averaged field generated by TF coils ($T$), PF coils ($P$), and the total vertical magnetic field (solid curve); (b) fields generated by the TF coils in the cross-section at the toroidal position of TF coils (1), between the TF coils (2), and toroidally averaged ($T$), as well as generated by PF coils (with the reversed sign, dashed curve).

tive estimation of the quality of the magnetic configuration we introduce the dimensionless aiming parameter, $\mu$, which combines the above requirements:

$$\mu = -100 W(\rho_m) \frac{\iota(\rho_m)}{\eta(\rho_m)} \frac{\rho_m}{r_c} \left(1 - \frac{\Delta R}{r_c}\right)^2 . \tag{8}$$

Here, $\rho_m$ is an average minor radius for the last closed flux surface, $r_c = D/2$ is a minor radius of a TF coil, and $\Delta R$ is a maximum shift of the magnetic axis relatively to the major radius of the TF coil center. The magnetic well, $W(\rho_m)$, and magnetic ripple, $\eta(\rho_m)$, are in percent. The normalization coefficient, 100, is introduced just to make $\mu$ to be of the order of 1 at the maximum. Figure 24 shows the aiming parameter, $\mu$, vs $\xi$ in the cases of independent variation of $N$, $\gamma$, $R$, and $r_c = D/2$. The apparent maximum of $\mu$ at $\xi \approx 1$ confirms our statement.

When parameter $\xi$ differs significantly from 1, the magnetic configuration is not optimal. At $\xi \gg 1$, as it was shown for $N$ variation in Sec. V, the flux surfaces from the external (internal) set shift farther from the TF coil center and closer to the outer (inner) current filament. The enclosed volume is reduced as well. For $\xi \ll 1$, the configuration is not optimal, mainly because of decreased rotational transform or increased magnetic ripple (see Sec. V).

### B. Rule 2 (the balance rule)

Let us consider $B_{zt}$—the total vertical magnetic field produced by the full coil system at some point in the equatorial plane of the device, and averaged over the toroidal direction, and $B_{zi}$ being the same, but for the magnetic field produced by the inclined TF coils only. Also, we consider the field, $B_{zp}$, which is the vertical magnetic field produced by the PF rings only, and taken at the same point of the equatorial plane.

Of course, these components are related, $B_{zt} = B_{zi} + B_{zp}$. The first part of the balance rule can be formulated as follows. In the region where closed flux surfaces exist, the component, $|B_{zt}|$, has to be significantly smaller than the component, $|B_{zi}|$, and the component, $|B_{zp}|$:

$$|B_{zt}| \ll |B_{zi}|, |B_{zp}|. \tag{9}$$

This rule means that the fields, $B_{zi}$ and $B_{zp}$, have to be of opposite sign, and they have to almost balance each other. We do not require the exact balance, $B_{zt} = 0$, because $B_{zt}$ is a function of the major radius of a point. Also, our experience shows that in the best cases the component $B_{zt}$, although small, was not exactly zero at any point in the region of the closed flux surfaces. To demonstrate this part of the rule, Fig. 25(a) shows the variation of $B_{zi}$ (curve with the symbol $T$), $B_{zp}$ (with the symbol $P$), and $B_{zt}$ (solid curve) with the major radius for our main case (the device in Fig. 7).

The second part of the balance rule considers $B_{zi1}$ and $B_{zi2}$ components of the vertical magnetic field generated by the inclined TF coils in the equatorial plane in the cross sections, respectively, at the toroidal position of TF coils and between the TF coils. Then the second part of the rule can be formulated as follows. In the region where the closed flux surfaces exist, the component, $B_{zp}$, generated by the poloidal field coils has to be intermediate between $B_{zi1}$ and $B_{zi2}$:

$$|B_{zi2}| < |B_{zp}| < |B_{zi1}|. \tag{10}$$

This rule is demonstrated in Fig. 25(b), prepared for the same parameters as before. The curves with the symbols 1, 2, and $T$, denote, respectively, the components $B_{zi1}$, $B_{zi2}$, and $B_{zi}$, while dashed curve shows the variation of $-B_{zp}$.

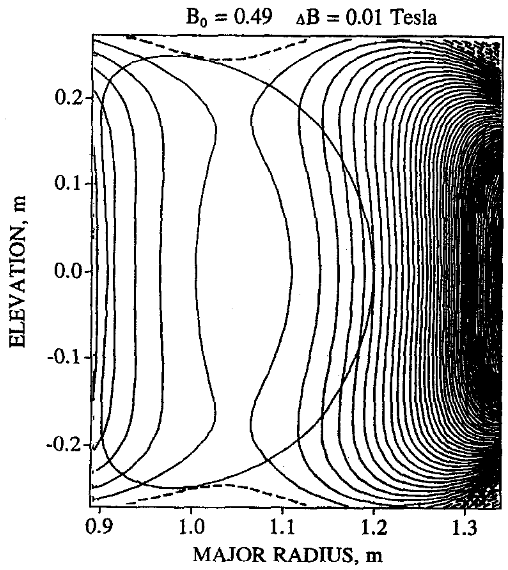


FIG. 26. Demonstration of the "location rule." Contours of $|B|$ for values larger than that at the magnetic axis are shown by the solid curves, and less than that at the magnetic axis—by the dashed curves. The last closed flux surface is presented as well. Numbers above the figure give the value of $|B|$ at the magnetic axis and the difference between the adjacent contour lines.

### C. Rule 3 (the location rule)

Results of many calculations show that in all cases when the magnetic configuration was close to the optimal one, the location of the magnetic axis, in the cross section corresponding to the toroidal position of TF coils, was close to the location of the saddle point of $|B|$ or to the location of the point of local minimum of $|B|$. Here, $|B|$ means the absolute value of the total magnetic field. To demonstrate this rule, Fig. 26 shows the $|B|$ distribution in the poloidal cross section at the toroidal position of TF coils for the same case as above. The contour lines are shown in Fig. 26, and the numbers above the plot give values of $B_0$, the magnetic field at the magnetic axis, and $\Delta B$, the separation between neighboring contour lines. The solid contour lines are drawn for $|B|>|B_0|$ and dashed lines for $|B|<|B_0|$.

These three rules are intended to help in the search of the acceptable configuration in the multidimensional parameter space. They still leave the significant degree of freedom in choosing of the TF and PF coil systems. Also, there is a relatively wide maximum around the working point defined by the above rules, and a good configuration can be found at the parameters somewhat different from the ones given by these rules. The configuration can be effectively optimized for the one particular parameter by sacrificing its optimization for a number of other parameters. In this case the configuration can also be somewhat different than that recommended by the above rules.

Any numerical example is necessarily concrete and prepared always for a particular set of parameters. A number of numerical examples presented above have been chosen for their simplicity and have been intended to demonstrate the general properties of the configuration with inclined coils. The scaling laws let one to extent the results obtained for one set of parameters to the other sets. Equation (7) can be viewed as a scaling law involving the main parameters, $R$, $N$, $D$, and $\gamma$: the configuration will be close to optimal if parameter $\xi$ stays close to 1. Some other scaling laws can be formulated as well. The magnetic configuration will be the same if all currents in all coils are multiplied by the same factor. The total local magnetic field will change by this factor, but the ratios between various components of the magnetic field vector will stay unchanged.

Some other useful relations between the currents and the parameters of the system have been discussed above in Sec. V (relation between PF coil currents and the inclination angle, $\gamma$ and relation between TF coil currents and a number of TF coils, $N$).

One more scaling is for spatial dimensions of the device: if all dimensions of the device (including all current-carrying coils) change by the same factor, $C$, the magnetic configuration will change to the similar one. Flux surface geometry and location of flux surfaces relative to the coils will be similar, the linear dimensions of flux surfaces change by the factor $C$, their surface areas—by the factor $C^2$, and the enclosed volumes—by the factor $C^3$. This scaling law is important, for example, for projection of the results obtained for a small device to the large one.

## VII. DISCUSSION AND CONCLUSIONS

In this paper, a configuration similar to the tokamak one but with the vertically inclined TF coils is analyzed. This device has the same system of planar coils (TF coils and PF coils) as a tokamak. However, inclination of the TF coils introduces a number of stellarator-like properties such as finite vacuum rotational transform and closed flux surfaces. These stellarator properties have been the main subject of this paper.

To understand why the inclined coils are able to create the stellarator effects, it is useful to find an analogy with the standard helical windings of the typical stellarator configuration. Let us divide each TF coil in two halves, the internal one and the external one. Combination of the external halves of the TF coils can be viewed as a part of the helical winding [see Fig. 27(a)]. Similar, the combination of the internal parts of the TF coils can be aligned with another helical winding having opposite helicity [Fig. 27(b)]. From this point of view, the optimization rule, formulated above, is becoming almost obvious: it corresponds to the best alignment with the imaginary helical windings, and hence, such a configuration can effectively generate helical harmonics of substantial amplitude. Each of this imaginary helical windings creates the magnetic structure similar to an $l=1$ stellarator. That is why the device with the inclined coils possesses two separate sets of the closed flux surfaces, one set (the external one) corresponds to the external parts of the TF coils, while another corresponds to their internal parts. Correspondingly, the internal and external sets have opposite helicity. Two separate sets of the closed flux surfaces is a unique peculiarity of the system considered. However, as it was found in Sec. IV, these two sets are not equal. Because of toroidicity, the external set is preferential for the optimization. It usually features a strong magnetic well and corresponds to larger en-

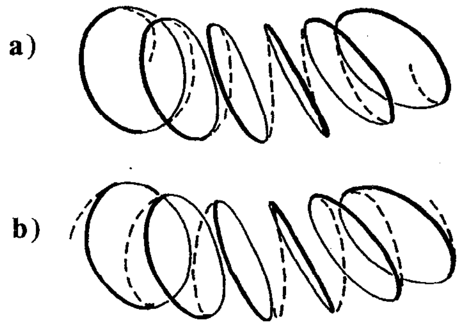


FIG. 27. Two helices, (a) and (b), with opposite helicity can be aligned with the same set of the inclined TF coils.

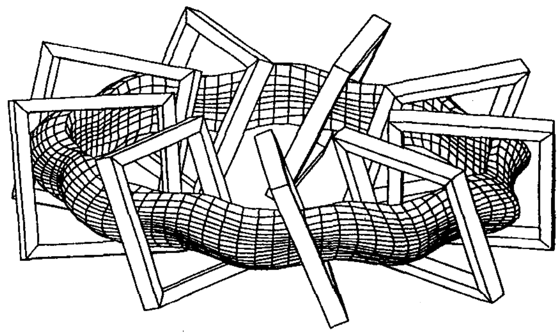

FIG. 28. Perspective view of the last closed flux surface in the system with rectangular TF coils.

closed volume and higher rotational transform, while the internal set has a magnetic hill in many cases.

Another important meaning can be given to the optimization rule, Eq. (7). Let us introduce the effective size, $D_0$, through the relation $D_0 = \pi R/N \sin \gamma$. If parameters of the device are not optimal and such that $D_0 \ll D$, then $D_0$ will be a characteristic size of the coil part that is participating in the generation of flux surfaces. Thus, there will be two such separate parts of the TF coil: the external part and the internal part of the coil. Moreover, the effective size, $D_0$, will be smaller for the internal part because the major radius, $R$, is smaller. The magnitude of $D_0$ approximately corresponds also to the effective size of the largest closed flux surfaces from these two sets. Again, because of toroidicity, the external set will have a larger enclosed volume. If one will change the parameters of the device in such a way that $D_0$ decreases while being less than $D$, then the visible effect will be the decrease of the size of the internal and external sets and shifting of these sets farther from each other and closer, respectively, to the internal and external parts of the TF coil. All these conclusions have been checked in our calculations.

The balance rule has a simple interpretation as well. It is clear that in the neighborhood of the magnetic axis one has to allow for the total vertical field, $B_z$, to change the sign. However, it is impossible if Eq. (9) is violated.

Two sets of the closed flux surfaces and all other effects considered above exist with the TF coils of different shapes. As examples, Fig. 28 shows the last closed vacuum flux surface produced by the rectangular TF coils, and Fig. 29—by the D-shaped TF coils (see also Ref. 24). Vacuum flux surfaces from the external sets are presented. As one can see, indeed, the different TF coils can be used to produce the stellarator-like effects, although the form factor can be substantial.

The studies of the vacuum magnetic configuration in devices with inclined TF coils show that such devices can be considered and used as the stellarator-type devices. However, we believe that the main advantages inherent to these devices, aside of their relative engineering simplicity, are in the possible applications to the tokamak configuration. This approach has significant potential for the tokamak improvement.

The process of transition from the currentless configuration, studied in this paper, to the standard tokamak configuration with the Ohmic current, will be a subject of separate analysis. Past experiments carried out on some stellarators with the Ohmic current (see, for example Refs. 35–37) give us confidence that we should not expect principal difficulties to appear during this transition to the tokamak regime.

Conclusions derived from the analysis presented in this paper and from the numerical computations of the magnetic field structure of the device with inclined TF coils can be formulated as follows.

Inclination of TF coils in a tokamak produces important stellarator-like properties: vacuum flux surfaces with significant rotational transform. A number of numerical examples have been considered to make it clear of how this device works. It was shown that the configuration can be optimized, and how the magnetic configuration changes when parameters differ from optimal.

Three rules—the optimization rule, the balance rule, and the location rule, useful for finding of the optimized configurations, have been obtained. Any numerical example is necessarily concrete and always prepared for a particular set of parameters. The scaling laws, formulated in Sec. VI, show one how to extend the results obtained for one set of parameters to the other sets of parameters.

The substantial role of the correct PF coil system is stressed, and it is shown that the PF system can be compensated, i.e., the total current can be zero. This can be impor-

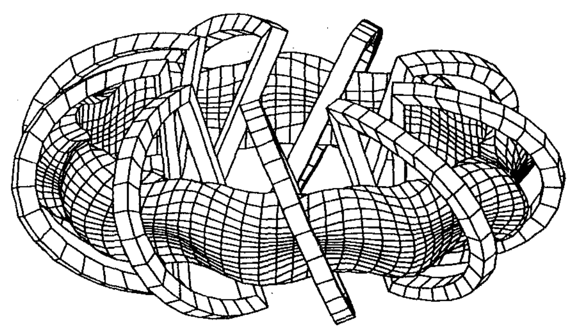

FIG. 29. Perspective view of the last closed flux surface in the system with D-shaped TF coils.

tant for tokamaks where the net current in the PF system might interfere with the performance of the Ohmic current transformer.

Two sets of the closed flux surfaces have been studied: the internal one and the external one. The analysis of the helical harmonic spectrum for these two sets showed that they have opposite helicity, i.e., the major helical harmonics are opposite. The field line traces represent opposite helices for these two sets as well. It was also shown that, because of finite toroidicity, the internal set is usually features a magnetic hill, while the external set has a magnetic well that is favorable for MHD stability. This peculiarity and some other advantages of the external set (larger enclosed volume and rotational transform) directed the main attention of our studies to the external set.

It was shown that the system of vertically inclined TF coils can effectively create the asymmetry in the helical harmonic spectrum. It was clarified that the main helical harmonic for the external set of closed flux surfaces is generated mainly by the external parts of the inclined TF coils, while that for the internal set is generated by the internal parts of these coils. Thus, the system of inclined TF coils has much in common with the two helical windings (helices) of opposite helicity. From this point of view, the optimization rule, which relates the four main parameters of the system, the major radius, the coil size, the number of coils, and the angle of inclination, corresponds to the best alignment between the TF coils and the corresponding helices.

It was shown that closed flux surfaces disappear in the limit of very high number of TF coils. Thus, toroidal inhomogeneity is a key factor, and the definite level of it is necessary for the closed flux surfaces of interest to exist. Inclination of the TF coils alone is not enough for the system to have the stellarator-like properties.

Although the configuration consisting of circular coils has been mainly studied in this paper, it was also checked that the different types of inclined TF coils can be used to create the stellarator-like effects. In particular, it was demonstrated that rectangular TF coils or D-shaped coils can generate vacuum flux surfaces as well.

The device with inclined TF coils possesses vacuum flux surfaces and vacuum rotational transform, and has a few potential advantages over the conventional tokamak. One of them is a non-Ohmic start-up of the discharge (with RF breakdown and RF plasma heating, for example) in such a device, that saves the available magnetic flux of the Ohmic current transformer to prolong the discharge. The non-Ohmic start-up to the relatively dense plasma means a possibility to simplify and improve of durability of the vacuum vessel and other toroidal construction elements of the tokamak, which, in this case, can be built without the isolating brakes. Because of additional rotational transform produced by the inclined TF coils, the device considered can be operated at lower plasma currents (for the same safety factor values). That means the reduction of energy released during disruptions and prolonged discharge operation (less Ohmic current is necessary). Also, the savings in the current drive power (required for the steady-state operation) can be significant.

Other possible applications are related to the problem of tearing mode stabilization and disruption control in tokamaks by introducing an additional helical magnetic field (see, for example, Refs. 35–38), which is readily available in the device with the inclined coils. Some other applications can be related to the problem of minimizing the magnetic field forces on TF coils[39] (especially if TF coils are superconducting[41]), which could be a critical issue for tokamaks utilizing extremely high magnetic fields.

## ACKNOWLEDGMENTS

The author would like to acknowledge contributions of many people to various subroutines that have been used in the UBFIELD code including those ones developed by Joseph Talmadge and David Anderson of the Torsatron/Stellarator Laboratory of the University of Wisconsin—Madison, and by J. Kisslinger of IPP, Garching. Valuable discussions with Joseph Talmadge and his cooperation in making all necessary subroutines available is greatly appreciated. Special thanks are due to Professor Noah Hershkowitz for his interest, support, and valuable discussions of this work. Various parts of the paper have been reported on weekly seminars of the Phaedrus Group and useful comments and suggestions from M. Kishinevsky, D. Brouchous, B. Breun, and other members of the Group are very appreciated. In particular, the comments of David Brouchous on the balance rule improved its formulation. The author would like also to acknowledge interesting discussions with A. V. Georgievskij.

This work was supported by U.S. Department of Energy Grant No. DE-FG02-88ER53264.

## APPENDIX: THE UBFIELD CODE

The code, UBFIELD, has been developed to study the magnetic field structure and search for the flux surfaces generated by the complicated coil system. In principle, it can treat arbitrary three-dimensional coils (including continuous helical windings) or any combination of various coils. In this paper we have mainly used the code to find and study the closed flux surfaces produced by the planar circular coils.

This code has not been written from scratch, but was based on the set of subroutines developed for a number of years at the Torsatron/Stellarator Laboratory of the University of Wisconsin—Madison by a number of people. New developments in the UBFIELD code include the following parts.

The UBFIELD code automatically controls all steps of the calculation, reading the data from the input file, transferring it from one subroutine to another, and sending results to the output file and graphics file. All graphics subroutines were written by using calls to the TV80 graphics library routines on CRAY. The convenient control over the device parameters from the input file simplifies the numerical building of the device. The numerous plots represent all stages of the calculating process. The output of the three-dimensional (3-D) view of the device, and its various cross sections help to control the correctness of the input parameters.

The search of the closed flux surfaces is programmed as a two stage process. First, the full spatial region under the search is divided into subregions, where the starting points are chosen. The code follows the magnetic field line originating from each starting point, and searches for the closed flux surfaces. The traces of these field lines are plotted. In case the closed flux surfaces are found, the second stage of the search can be initiated. During the second stage of the search the code finds the magnetic axis and is trying to find as many closed flux surfaces as it can by increasing the minor radius by a given step. This search continues till the field line goes beyond the search area.

The code calculates and makes graphics output for the variation of magnetic field, **B**, along the field line for every flux surface found. It calculates the volume of the magnetic flux surface and the average minor radius and plots the rotational transform, the magnetic ripple, and the magnetic well as functions of the average minor radius. The flux surfaces found are analyzed for the helical harmonic spectrum as well.

The full coil system and the largest flux surface are represented then as a set of quadrilaterals, which is a necessary process for the perspective 3-D view plotting with the hidden lines removed.

The UBFIELD code is a very fast one because the subroutines, it is based on, utilize various analytical formulas instead of the direct calculation of the magnetic field from the Biot–Savart law. For this paper it probably would be relevant to mention only the formulas for the magnetic field generated by the circular coil. Such calculations have been done through the complete elliptic integrals $K$ and $E$.[42] In the Cartesian coordinate system where the coil center has coordinates (0,0,0) and the coil of the radius, $a$, with the current, $I$, is located in the $(x,y)$ plane, the magnetic field at the arbitrary point $(x,y,z)$ can be expressed as follows:

$$B_x=\frac{x}{d}\,B_d, \tag{A1}$$

$$B_y=\frac{y}{d}\,B_d, \tag{A2}$$

$$B_z=C\left(K(k^2)+\frac{a^2-r^2}{(a-d)^2+z^2}\,E(k^2)\right), \tag{A3}$$

where

$$B_d=C\,\frac{z}{d}\left(-K(k^2)+\frac{a^2+r^2}{(a-d)^2+z^2}\,E(k^2)\right), \tag{A4}$$

and

$$k^2=\frac{4ad}{(a+d)^2+z^2}, \tag{A5}$$

$$d=\sqrt{x^2+y^2}, \tag{A6}$$

$$r^2=d^2+z^2, \tag{A7}$$

$$C=\frac{\mu_0 I}{2\pi}\,\frac{1}{\sqrt{(a+d)^2+z^2}}, \tag{A8}$$

and $\mu_0$ is a free space permeability.

To model the finite width of the TF and PF coils, a combination of four nearby current filaments, each one with one-quarter of the total current, has been used in the code for all results presented in this paper.

Because the UBFIELD code is fast, we were able to check that closed flux surfaces remain to be closed for the large number of revolutions of the field line around the torus. Integration along the field line for one field period, $\Delta\varphi=2\pi/N$ ($N$ is a number of field periods), adds one point to the flux surface cross section for each cross section of interest. A typical number of points in our calculations representing each closed flux surface was between 500 and 1500.

In some cases, usually when the flux surface was too close to the separatrix and the angle of inclination was large, the notable island structure has been found. These "bad" flux surfaces have not been included into the sets of closed flux surfaces presented in this paper.


[1] J. Jacquinot, V. P. Bhatnagar, C. Gormezano, and the JET Team, Plasma Phys. Controlled Fusion A **35**, 35 (1993).
[2] R. J. Hawryluk and the TFTR Team, "Review of recent D–T experiments from TFTR," *Proceedings of the 15th IAEA Conference of Plasma Physics and Controlled Nuclear Fusion Research, Seville* (International Atomic Energy Agency, Vienna, in press).
[3] M. Mori, S. Ishida, T. Ando, K. Annoh, N. Asakura, M. Azumi, A. A. van Blokland, G. J. Frieling, T. Fujii, T. Fujita, T. Fukuda, A. Funahashi, T. Hatae, M. Hoek, M. Honda, N. Hosogane, N. Isei, K. Itami, Y. Kamada, Y. Kawano, M. Kikuchi, H. Kimura, T. Kimura, H. Kishimoto, A. Kitsunezaki, K. Kodama, Y. Koide, T. Kondoh, H. Kubo, M. Kuriyama, M. Matsuoka, Y. Matsuzaki, N. Miya, M. Nagami, A. Nagashima, O. Naito, H. Nakamura, M. Nemoto, Y. Neyatani, H. Ninomiya, T. Nishitani, T. Ohga, S. Ohmori, M. Saidoh, A. Sakasai, M. Sato, M. Shimada, K. Shimizu, H. Shirai, T. Sugie, H. Takeuchi, K. Tani, K. Tobita, S. Tsuji, K. Ushigusa, M. Yamada, I. Yonekawa, H. Yoshida, and R. Yoshino, Nucl. Fusion **34**, 1045 (1994).
[4] J. F. Lyon, Fusion Technol. **17**, 19 (1990).
[5] B. A. Carreras, G. Grieger, J. H. Harris, J. L. Johnson, J. F. Lyon, O. Motojima, F. Rau, H. Renner, J. A. Rome, K. Uo, M. Wakatani, and H. Wobig, Nucl. Fusion **28**, 1613 (1988).
[6] V. A. Batyuk, S. E. Grebenshchikov, I. A. Kovan, A. I. Meshcheryakov, P. E. Moroz, I. S. Sbitnikova, V. N. Sukhodol'sky, and I. S. Shpigel, *Proceedings of the 3rd Joint Varenna–Grenoble International Symposium on Heating in Toroidal Plasmas*, Grenoble, France, 1982, edited by C. Gormezano, G. G. Leotta, and E. Sindoni (Commissariat a'l'Energie Atomique, Paris, 1982), Vol. 2, p. 273.
[7] L. M. Kovrizhnykh and P. E. Moroz, Sov. Phys. Tech. Phys. **9**, 735 (1983).
[8] V. E. Bykov, A. V. Georgievskij, V. V. Demchenko, Yu. K. Kuznetsov, Yu. A. Litvinenko, A. V. Longinov, O. S. Pavlichenko, V. A. Rudakov, K. N. Stepanov, and V. T. Tolok, Fusion Technol. **17**, 140 (1990).
[9] J. F. Lyon, B. A. Carreras, K. K. Chipley, M. J. Cole, J. H. Harris, T. C. Jernigan, R. L. Johnson, V. E. Lynch, B. E. Nelson, J. A. Rome, J. Sheffield, and P. B. Thompson, Fusion Technol. **10**, 179 (1986).
[10] J. F. Lyon, G. L. Bell, R. D. Benson, T. S. Bigelow, K. K. Chipley, R. J. Colchin, M. J. Cole, E. C. Crume, J. L. Dunlap, A. C. England, J. C. Glowienka, R. H. Goulding, J. H. Harris, D. L. Hillis, S. Hiroe, L. D. Horton, H. C. Howe, R. C. Isler, T. C. Jernigan, R. L. Johnson, R. A. Langley, M. M. Menon, P. K. Mioduszewski, R. N. Morris, M. Murakami, G. H. Neilson, B. E. Nelson, D. A. Rasmussen, J. A. Rome, M. J. Saltmarsh, P. B. Thompson, M. R. Wade, J. A. White, T. L. White, J. C. Whitson, J. B. Wilgen, and W. R. Wing, Fusion Technol. **17**, 33 (1990).
[11] G. H. Neilson and J. H. Harris, Nucl. Fusion **27**, 711 (1987).
[12] T. Obiki, M. Wakatani, M. Sato, S. Sudo, F. Sano, T. Mutoh, K. Itoh, K. Kondo, M. Nakasuga, K. Hanatani, H. Zushi, T. Mizuuchi, H. Kaneko, H. Okada, Y. Takeiri, Y. Nakamura, S. Besshou, Y. Ijiri, M. Iima, T. Senju, K. Yaguchi, T. Baba, and S. Kobayashi, Fusion Technol. **17**, 101 (1990).
[13] A. Iiyoshi, M. Fujiwara, O. Motojima, N. Ohyabu, and K. Yamazaki, Fusion Technol. **17**, 169 (1990).
[14] J. Sapper and H. Renner, Fusion Technol. **17**, 63 (1990).
[15] C. Beidler, G. Grieger, F. Herrnegger, E. Harmeyer, J. Kisslinger, W. Lotz, H. Maassberg, P. Merkel, J. Nuhrenberg, F. Rau, J. Sapper, F. Sardei, R.

Scardovelli, A. Schluter, and H. Wobig, Fusion Technol. **17**, 148 (1990).
[16]D. T. Anderson, A. F. Almagri, F. S. B. Anderson, P. G. Matthews, J. L. Shohet, and J. N. Talmadge, Bull. Am. Phys. Soc. **39**, 1601 (1994).
[17]C. Alejaldre, J. J. Gozalo, J. B. Perez, F. C. Magana, J. R. Diaz, J. G. Perez, A. Lopez-Fraguas, L. Garcia, V. I. Krivenski, R. Martin, A. P. Navarro, A. Perea, A. Rodriguez-Yunta, M. S. Ayza, and A. Varias, Fusion Technol. **17**, 131 (1990).
[18]S. M. Hamberger, B. D. Blackwell, L. E. Sharp, and D. B. Shenton, Fusion Technol. **17**, 123 (1990).
[19]M. G. Shats, D. L. Rudakov, B. D. Blackwell, L. E. Sharp, R. Tumlos, and S. M. Hamberger, *Proceedings of the 21st European Conference on Controlled Fusion and Plasma Physics*, Montpellier, 1994 (European Physical Society, Petit-Lancy, Switzerland, 1994), p. 150.
[20]J. Kisslinger, *Proceedings of the Workshop on W VII-X*, Schloss Ringberg, 1987 (Commission of the European Communities, Brussels, 1987), p. 145.
[21]V. E. Bykov, E. D. Volkov, A. V. Georgievskij, Yu. K. Kuznetsov, S. A. Martynov, V. G. Peletminskaya, K. S. Rubtsov, V. A. Rudakov, Yu. F. Sergeev, A. V. Khodyachikh, and A. A. Shishkin, *Proceedings of the 12th IAEA International Conference on Plasma Physics and Controlled Nuclear Fusion Research*, Nice, 1988 (International Atomic Energy Agency, Vienna, 1989), Vol. 2, p. 403.
[22]A. V. Georgievskij, S. A. Martynov, V. A. Rudakov, Yu. F. Sergeev, and A. V. Khodyachikh, Vopr. Atomn. Nauki Tekh., Ser. Termoyad. Sintez **4**, 28 (1989) (in Russian).
[23]V. E. Bykov, E. D. Volkov, V. P. Vorobiova, A. V. Georgievskij, Yu. K. Kuznetsov, S. A. Martynov, V. F. Peletminskaya, V. A. Rudakov, Yu. F. Sergeev, M. A. Khatzhmuradov, and A. V. Khodyachikh, *Proceedings of the IAEA Technical Committee Meeting and 8th Stellarator Workshop*, Kharkov, 1991 (International Atomic Energy Agency, Vienna, 1991), p. 441.
[24]A. V. Georgievskij, S. A. Greek, A. I. Lysojvan, V. E. Moiseenko, I. S. Pinchuk, V. A. Rudakov, V. V. Nemov, and M. A. Khadzhmuradov, *Proceedings of the IAEA Technical Committee Meeting Stellarators and Other Helical Conference Systems*, Garching, 1993 (International Atomic Energy Agency, Vienna, 1993), p. 480.
[25]A. H. Boozer, T. K. Chiu, R. L. Dewar, H. P. Furth, J. A. Goree, J. L. Johnson, R. M. Kulsrud, D. A. Monticello, G. Kuo-Petravic, G. V. Sheffield, S. Yoshikawa, and O. Betancourt, *Proceedings of the 9th IAEA International Conference on Plasma Physics and Controlled Nuclear Fusion Research*, Baltimore, 1982 (International Atomic Energy Agency, Vienna, 1983), Vol. III, p. 129.
[26]S. N. Popov and A. P. Popryaduhin, Sov. Phys. Tech. Phys. **11**, 284 (1966).
[27]M. A. Ivanovsky, S. N. Popov, and A. P. Popryaduhin, in *Stellarators*, edited by D. B. Skobel'tsin (Trudy FIAN, Nauka, Moscow, 1973), Vol. 65, p. 65 (in Russian).
[28]S. Rehker and H. Wobig, *Proceedings of the 6th European Conference on Controlled Fusion and Plasma Physics*, Moscow, 1973 (European Physical Society, Petit-Lancy, Switzerland, 1973) Vol. 1, p. 117.
[29]A. V. Georgievskij, V. E. Ziser, V. V. Nemov, V. G. Peletminskaya, D. P. Pogozhev, Yu. F. Sergeev, M. N. Skoblik, and A. A. Shishkin, Nucl. Fusion **14**, 79 (1974).
[30]A. Reiman and A. Boozer, Phys. Fluids **26**, 3167 (1983).
[31]R. Majeski, P. Probert, P. Moroz, T. Intrator, R. Breun, D. Brouchous, H. Y. Che, J. R. DeKock, D. Diebold, M. Doczy, R. Fonck, N. Hershkowitz, R. D. Johnson, M. Kishinevsky, G. McKee, J. Meyer, P. Nonn, S. P. Oliva, J. Pew, J. Sorensen, T. Tanaka, M. Vukovic, and G. Winz, Phys. Fluids B **5**, 2506 (1993).
[32]N. Hershkowitz, P. Moroz, P. Probert, E. Y. Wang, T. Intrator, D. Diebold, R. Breun, D. Brouchous, M. Doczy, D. Edgell, A. Elfimov, R. Fonck, M. Kishinevsky, C. Litwin, P. Nonn, S. Regan, J. Sorensen, J. Tataronis, M. Vukovic, X. Wang, and S. Wukitch, "Alfven wave current drive and heating," in Ref. 2.
[33]R. D. Stambaugh and the DIII-D Team, *Proceedings of the 13th IAEA International Conference on Plasma Physics and Controlled Nuclear Fusion Research*, Washington DC, 1990 (International Atomic Energy Agency, Vienna, 1991), Vol. 1, p. 69.
[34]M. Porkolab, R. Boivin, F. Bombarda, P. Bonoli, C. Christensen, D. Garnier, S. Fairfax, C. Fiore, J. Goetz, S. Golovato, M. Graf, R. Granetz, M. Greenwald, D. Gwinn, S. Horne, T. Hsu, A. Hubbard, I. Hutchinson, J. Irby, D. Jablonski, C. Kurz, B. LaBombard, B. Lipschultz, T. Luke, E. Marmar, M. May, A. Mazurenko, G. McCracken, R. Nachtrieb, A. Niemczewski, P. O'Shea, J. Reardon, J. Rice, J. Schachter, J. Snipes, J. Sorci, P. Stek, Y. Takase, J. Terry, G. Tinios, J. Urbahn, Y. Wang, R. Watterson, B. Welch, and S. Wolfe, "Overview of recent results from Alcator C-Mod," in Ref. 2.
[35]D. V. Bartlett and the W VII-A Team, Nucl. Fusion **20**, 1093 (1980).
[36]J. Fujita, S. Itoh, K. Kadota, K. Kawahata, Y. Kawasumi, O. Kaneco, T. Kuroda, K. Matsuoka, K. Matsuura, K. Miyamoto, N. Noda, Y. Oka, K. Ohkubo, K. Sakurai, K. Sato, M. Sato, S. Tanahashi, Y. Terashima, and K. Toi, *Proceedings of the 8th IAEA Conference on Plasma Physics and Controlled Nuclear Fusion Research*, Brussels, 1980 (International Atomic Energy Agency, Vienna, 1981), Vol. 1, p. 209.
[37]E. D. Andryukhina, M. S. Berezhetskij, M. A. Blokh, G. S. Voronov, S. E. Grebenshchikov, N. P. Donskaya, K. S. Dyabilin, B. I. Kornev, S. V. Kladov, L. M. Kovrizhnykh, N. F. Larionova, N. V. Lunin, S. N. Popov, M. S. Rabinovich, I. S. Sbitnikova, Y. V. Kholnov, A. V. Khudoleev, O. I. Fedyanin, I. S. Shpigel, and S. V. Shchepetov, in Ref. 36, p. 199.
[38]M. I. Michajlov and V. D. Shafranov, Nucl. Fusion **30**, 413 (1990).
[39]A. V. Georgievskij (private communication, 1995).
[40]L. S. Solov'ev and V. D. Shafranov, in *Reviews of Plasma Physics*, edited by M. A. Leontovich (Consultants Bureau, New York, 1970), Vol. 5, p. 1.
[41]R. J. Thome, M. Huguet, and the ITER Joint Central Team and Home Teams, "Superconducting magnets: Major design and R&D issues and ITER," in Ref. 2.
[42]M. Abramowitz and I. A. Stegun, in *Handbook of Mathematical Functions with Formulas, Graphs and Mathematical Tables* (National Bureau of Standards, Washington, DC, 1964), Chap. 17.